Ultramicroscopy 136 (2014) 31–41

Contents lists available at ScienceDirect

Ultramicroscopy

journal homepage: www.elsevier.com/locate/ultramic

Enhanced light element imaging in atomic resolution scanning transmission electron microscopy

S.D. Findlay [a,*], Y. Kohno [b], L.A. Cardamone [a], Y. Ikuhara [c,d,e], N. Shibata [c,f]

[a] School of Physics, Monash University, Victoria 3800, Australia
[b] JEOL Ltd., Tokyo 196-8558, Japan
[c] Institute of Engineering Innovation, School of Engineering, University of Tokyo, Tokyo 113-8656, Japan
[d] Nanostructures Research Laboratory, Japan Fine Ceramics Center, Nagoya 456-8587, Japan
[e] WPI Advanced Institute for Materials Research, Tohoku University, Sendai 980-8577, Japan
[f] PRESTO, Japan Science and Technology Agency, Saitama 332-0012, Japan

ARTICLE INFO

Article history:
Received 28 May 2013
Received in revised form
21 July 2013
Accepted 25 July 2013
Available online 2 August 2013

Keywords:
Scanning transmission electron microscopy (STEM)
Atomic resolution imaging
Annular bright field (ABF)

ABSTRACT

We show that an imaging mode based on taking the difference between signals recorded from the bright field (forward scattering region) in atomic resolution scanning transmission electron microscopy provides an enhancement of the detectability of light elements over existing techniques. In some instances this is an enhancement of the visibility of the light element columns relative to heavy element columns. In all cases explored it is an enhancement in the signal-to-noise ratio of the image at the light column site. The image formation mechanisms are explained and the technique is compared with earlier approaches. Experimental data, supported by simulation, are presented for imaging the oxygen columns in $LaAlO_3$. Case studies looking at imaging hydrogen columns in YH_2 and lithium columns in Al_3Li are also explored through simulation, particularly with respect to the dependence on defocus, probe-forming aperture angle and detector collection aperture angles.

1. Introduction

The scientific and technological importance of light elements in a diverse range of materials – oxygen in cuprate superconductors, lithium in battery materials, hydrogen in hydrogen-storage materials, to name but three – makes imaging of these elements highly desirable in materials characterization. For atomic resolution structure analysis, annular dark field (ADF) imaging in scanning transmission electron microscopy (STEM) has long provided robust and directly interpretable images, but the thermal-scattering-dominated contrast strongly favours heavy elements [1]. ADF has recently been complemented by the development of annular bright field (ABF) imaging [2–4], involving an annular detector in the outer area of the bright field (forward scattering region) and enabling the simultaneous imaging of light and heavy elements with similar contrast. A similar recent and closely related approach, middle-angle bright field (MaBF)[1] imaging [5], involves an on-axis disk detector with outer angle about half (hence "middle") the probe-forming aperture angle and shows light and heavy elements with opposite contrast but consequently better resolution. MaBF and ADF images can be combined into colour composite images to aid visual interpretation [6].

Though not without precedent in the earlier literature, the usage of an annular detector in or near the bright field having been much explored [7–9], the newfound appreciation that for atomically fine probes ABF imaging enabled robust visualization of light elements over a wide thickness range led to its rapid uptake through the field [10–21]. The direct ABF imaging of lithium [22–30] and of hydrogen [31,32] within crystalline matrices using STEM is of particular note because of the technological interest in lithium-bearing materials for lithium-battery devices and hydrogen-bearing materials for hydrogen storage applications. Nevertheless, ABF of these very light elements remains challenging. Light-element-bearing specimens tend to damage under the electron beam, but trying to avoid this by reducing the dose reduces the signal-to-noise ratio. Moreover, ABF imaging of very light elements anyway involves looking for a small signal, a slight intensity dip, which may be of comparable magnitude to scattering artefacts or to noise, on a large background. Techniques which improve the signal, either by enhancing the signal in an absolute sense or by minimizing the dose via recording as many scattered electrons as possible [33], will be an asset to materials characterization. In this paper we show that the *difference* between the ABF and MaBF images, which for convenience we refer to as enhanced ABF (eABF) imaging, is such a technique.

* Corresponding author. Tel.: +61 3 9902 4943; fax: +61 3 9905 3637.
E-mail address: scott.findlay@monash.edu (S.D. Findlay).

[1] We have taken the liberty of using a lower case "a" in MaBF to emphasise that it does not abbreviate the same word as the "A" in ABF and ADF.

0304-3991/$ - see front matter © 2013 Elsevier B.V. All rights reserved.
http://dx.doi.org/10.1016/j.ultramic.2013.07.019

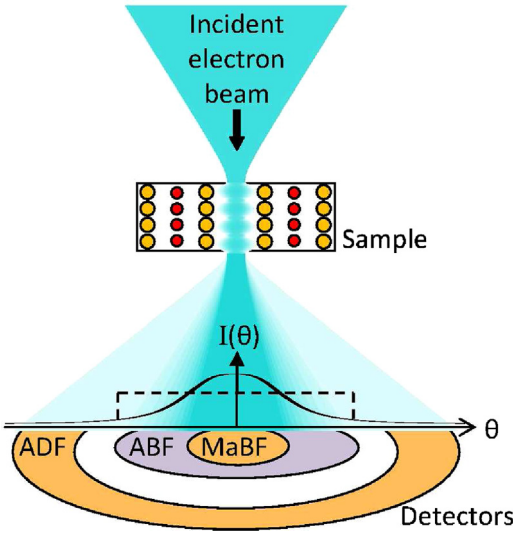

Fig. 1. Schematic of some key detector geometries in atomic resolution STEM.

2. Conceptual background

It is useful to first develop an intuitive understanding of ABF and MaBF imaging. Fig. 1 shows a schematic of the electron probe "channelling" (scattering) along a column of atoms and the resultant intensity profile in the diffraction pattern as a function of angle θ away from the optical axis. In the absence of a sample, the diffraction profile would be a top-hat function (dashed line) spanning the bright field. Scattering through a sample redistributes this intensity (solid line). The real intensity distribution would likely have finer structural features, but the general behaviour – the intensity increased in the inner area of the bright field, reduced in the outer area of the bright field, and spreading out into the dark field – is correct for atomically fine probes atop relatively light columns. Atop heavier columns, a larger portion of electrons are scattered into the dark field, reducing the intensity throughout the bright field. That both mechanisms lead to a reduced intensity in the outer area of the bright field over a wide range of elements and sample thicknesses is the basis of the robust, absorptive form of ABF images. That the intensity tends to peak up in the forward direction for light element columns (where channelling dominates over thermal scattering) but reduces for heavy element columns (where thermal scattering dominates over channelling) is the basis for the mixed-contrast form of MaBF images. A more rigorous derivation of this behaviour on an individual column basis and using the s-state model [34] has been given by Findlay and colleagues [3,4] and a full Bloch state analysis for MaBF imaging has been given by Ohtsuka et al. [5].

By way of example, ADF, ABF and MaBF images of $LaAlO_3$ viewed along the [001] direction as a function of specimen thickness are compared in Fig. 2(a)–(c) (parameters are given in the figure caption; structural data taken from Ref. [35]). For each mode, the top half of the panel assumes an infinitesimal/point effective source size (i.e. perfect spatial coherence) while the lower half, more realistically, assumes a finite, incoherent effective source described via a Gaussian of half-width 0.05 nm [36], both, of course, subjected to the diffraction limit of the probe-forming lens. As expected, the ADF images in Fig. 2(a) are dominated by the heavy La column, with the Al/O column faintly visible but the O columns invisible. The ABF images assuming perfect spatial coherence, the top half of Fig. 2(b), show all columns – La, Al/O and pure O – consistent with the previously touted utility of ABF for imaging light elements. However, when spatial incoherence is taken into account in the bottom half of Fig. 2(b), the O columns are only weakly visible for a small subset

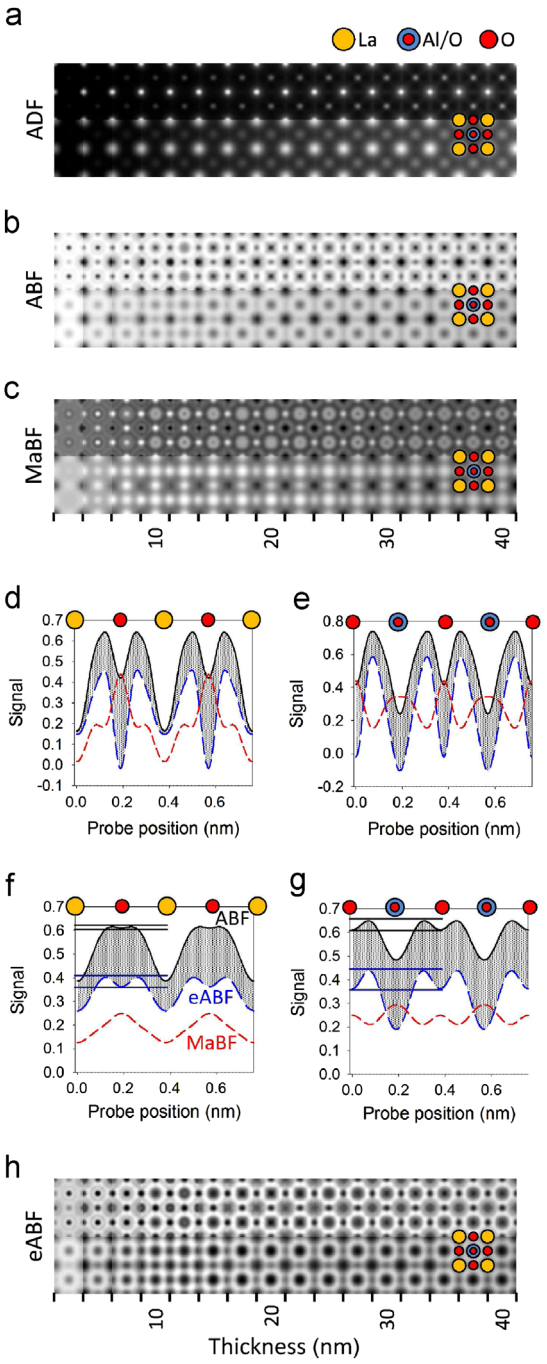

Fig. 2. (a) ADF, (b) ABF and (c) MaBF images as a function of thickness for $LaAlO_3$ viewed along the [001] direction for a 200 keV probe with a 23 mrad probe-forming aperture angle. The detector ranges are ADF 81–228 mrad; ABF 11.5–23 mrad; MaBF 0–11.5 mrad. The upper half of each panel assumes perfect spatial coherence, while the lower half incorporates a Gaussian incoherent effective source of half-width 0.05 nm. (d) and (e) show line profiles, assuming a 20 nm thick sample, through the alternating La–O–La column sequence and the alternating O–Al/O–O column sequence, respectively, for perfect coherence, while (f) and (g) show the same profiles assuming a Gaussian incoherent effective source of half-width 0.05 nm. The grey shading between the ABF and eABF profiles emphasises the relative enhancement of the visibility in the pure O columns in the latter over the former. The horizontal lines in (f) and (g) provide a guide to the eye of the change in local visibility of the O column between ABF and eABF images. (h) eABF images, being the difference between the images in (b) and (c). (For interpretation of the references to colour in this figure caption, the reader is referred to the web version of this article.)

of specimen thicknesses. The MaBF images assuming perfect spatial coherence, the top half of Fig. 2(c), show pure O columns bright and La columns dark, while the contrast of the Al/O column is thickness